Green Chemistry

Accepted Manuscript

This article can be cited before page numbers have been issued, to do this please use: L. Qi, Z. Luo and X. Lu, *Green Chem.*, 2019, DOI: 10.1039/C9GC00779B.

ROYAL SOCIETY OF CHEMISTRY

rsc.li/green-chem

View Article Online
DOI: 10.1039/C9GC00779B

Modulation of starch nanoparticles surface characteristics for facile construction of recycling Pickering interfacial enzymatic catalysis

Liang Qi[1], Zhigang Luo[1,2,3]*, Xuanxuan Lu[4]

1. School of Food Science and Engineering , South China University of Technology, Guangzhou, 510640, China.

2.South China Institute of Collaborative Innovation, Dongguan, 523808, China.

3.Overseas Expertise Introduction Center for Discipline Innovation of Food Nutrition and Human Health (111 Center), Guangzhou 510640, China.

4.Department of Food Science, Rutgers, The State University of New Jersey, 65 Dudley Rd, New Brunswick, New Jersey 08901, USA.

*Corresponding author:

Zhigang Luo, Tel: +86-20-87113845, Fax: +86-20-87113848. *E-mail address*: *zhgluo@scut.edu.cn*

View Article Online
DOI: 10.1039/C9GC00779B

Abstract

In this work, maize starch (MS) was successively modified via the esterification reaction with acetic anhydride (AA) and phthalic anhydride (PTA). Combined with the gelatinization-precipitation process, the formed starch nanoparticles at AA/PTA ratio of 2 (MS-AP (2)) and 3 (MS-AP (3)) had the similar regular spheres but distinct surface characteristics. In order to enhance the activity of lipase B from *Candida antarctica* (CALB) in organic solvent, we designed oil-in-water (o/w) and water-in-oil (w/o) Pickering interfacial catalytic system simultaneously by utilizing MS-AP (2) and MS-AP (3) as robust Pickering emulsion stabilizers. Impressively, in the esterification of 1-butanol and vinyl acetate, the specific activity of CALB in the o/w ($0.0843 U \cdot \mu L^{-1}$) or w/o ($0.0724 U \cdot \mu L^{-1}$) Pickering interfacial catalytic system was much higher than that of free enzymes in the monophasic ($0.0198 U \cdot \mu L^{-1}$) and biphasic ($0.0282 U \cdot \mu L^{-1}$) system. Meanwhile, after preliminarily elaborating mass transfer discrepancies between o/w and w/o Pickering interfacial catalytic system and calculating their mass transfer resistance, we clarified the effects of the location of two phases on the catalytic capacity of Pickering emulsion. Impressively, both Pickering interfacial catalytic systems exhibited high effectiveness in product separation. It was found that w/o Pickering emulsion enabled the organic

View Article Online
DOI: 10.1039/C9GC00779B

product to be facilely isolated through a simple decantation, while o/w Pickering emulsion achieved the same results after adjusting system temperature. The biobased nanomaterials and simple protocol, in conjunction with the stability to simultaneously achieve high catalysis efficiency and excellent recyclability, makes us believe that this starch nanoparticles-based Pickering interfacial catalytic system is promising for meeting the requirements of green and sustainable chemistry.

Key words: Starch nanoparticles, Pickering emulsion, interfacial enzymatic catalysis, recyclable catalysis, green and sustainable chemistry.

Introduction

Enzymes catalyze a broad variety of organic reactions with high chemo-, stereo-, and regioselectivity under mild conditions[1]. However, the application of free enzymes in organic media is often hampered by the fact that, in many cases, enzymes have low stability and poor recyclability. A simple, gentle, and general way to solve these problems is to create a microenvironment to maintain the enzyme activity in biphasic aqueous-organic system[2]. In recent years, such researches have advanced in a promising direction toward the use of nanoparticles as building blocks for the construction of capsules (often referred to as Pickering emulsions) as enzyme carriers[3-6]. The presence of Pickering emulsion droplets in the reaction systems can

View Article Online
DOI: 10.1039/C9GC00779B

significantly accelerate organic/aqueous biphasic reactions because a large liquid-solid interfacial area is created. To meet above requirements, it takes hydrophobic modification of nanoparticle surface to construct water-in-oil (w/o) Pickering emulsion. Meanwhile, high interfacial activity is necessary for nanoparticles to be closely packed at the oil-water interface. Moreover, the biocompatibility of nanoparticles to enzymes as another crucial parameter has to be considered[7]. As a result, elaborately modified synthetic stabilizers, involving hybrid micelles[8, 9], polymersomes[6, 10] and surface functionalized inorganic particles[11-13], have been reported in the Pickering interfacial enzymatic catalysis.

As we know, once the particles are anchored onto the emulsion droplet surface, they cannot optionally depart from the droplet surface due to a high energy barrier[14]. Therefore, the applications of oil-in-water (o/w) Pickering emulsion are hampered in enzymatic catalysis because existing methods for product separation, such as heating and centrifugation, are bothersome due to enzyme activity loss, high time- and energy-consumption. Inspired by interfacial metal nanoparticles catalysis[15-17], we propose developing stimulus-responsive o/w Pickering emulsions is a potential way, because stimulus-responsive demulsification/emulsification cycle or phase inversion provides a good recyclability and a facile separation. To meet this requirement,

View Article Online
DOI: 10.1039/C9GC00779B

surface charge, wettability and even size that governs the stabilizer performance, are required to be easily tuned by adjusting the surrounding environment stimulation factors[18]. However, since the transformation of environment stimulation factors is dramatic in these reports, which may not be suitable for preserving the enzyme activity, few stimulus-responsive o/w Pickering emulsions have been reported in interfacial enzyme catalysis until now. Therefore, this limitation urges the development of modified nanoparticles that are sensitive to the environment stimulation factors.

In recent years, starch nanoparticles have acquired a reputation as having potential as biobased nanomaterials since they are easily processed, renewable, biocompatible, and nontoxic.[19] Notably, they have been intensively studied as stabilizers for Pickering emulsions owing to their regular sphere shape and excellent tolerance in both organic and water phase. [20, 21]Moreover, the abundant hydroxyls endows starch with a reaction activity, thus esterifying agent, alkyl chains and polymer chains can be easily introduced on the starch chains through hydroxyls-derived reactions.[22, 23] In this way, it is easy to functionalize the starch nanoparticles to acquire the interfacial activity and structural characteristics as requested.

View Article Online
DOI: 10.1039/C9GC00779B

The starch modification with acetic anhydride (AA) has been reported to reduce surface energy of starch nanocrystals[24] or cellulose nanofibers[25] and shows a good solubility in organic solvents such as acetone, chloroform and ethyl acetate. Because of unique hydrophobicity, acetylated starch nanocrystals are useful in applications in packaging industry and as nano-reinforcements[24]. Meanwhile, phthalic anhydride (PTA) is a preferred esterifying agent, which displays the pH-responsive property with sensitive protonation-deprotonation transition of carboxyl[20, 26]. By adjusting the pH values, its charged-uncharged interconversion impacts the surface wettability of attached substrates. Based on this, through the adjustment of substitution degrees of AA and PTA, it is expected to modulate the surface characteristics of starch nanoparticles and achieve the hydrophilic and hydrophobic starch nanoparticles with high interfacial activity simultaneously. Accordingly, hydrophobic starch nanoparticle can be a potential candidate for the interfacial enzymatic catalysis in w/o Pickering emulsion. In the meantime, the presence of PTA gives an opportunity for hydrophilic starch nanoparticles to construct stimulus-responsive o/w Pickering emulsions applying to the interfacial enzymatic catalysis.

Besides, it is worth noting that, for the synthesis of starch nanoparticles, the traditional acid hydrolysis is not an option under the ever-growing environmental

View Article Online
DOI: 10.1039/C9GC00779B

pressure. Delightfully, the process of nanoprecipitation has been investigated as a new procedure for the generation of nanoparticles[27, 28]. This process involves the successive addition of a dilute solution of polymer to a nonsolvent, which leads to polymer precipitation at a nanoscale. Benefiting from this, starch possesses a higher chemical activity by liberalizing the molecular chains to expose more active hydroxyl groups, and the usage of large amounts of toxic solvents and external energy sources are avoided, which is in accordance with environment-friendly concept.

Herein, through optimizing the rational adjustments of AA and PTA substitution degree and cooperation with the gelatinization-precipitation method, we synthesized two starch nanoparticles with the similar regular spheres but distinct surface characteristics. The structure of starch nanoparticles was clarified using ^{1}H nuclear magnetic resonance (^{1}H NMR), the results from X-ray diffraction (XRD) and scanning electron microscopy (SEM) disclosed the change of crystallinity, morphology and size of nanoparticles at different degree of esterification. For enhancing lipase activity in organic solvent, we designed oil-in-water (o/w) and water-in-oil (w/o) Pickering interfacial catalytic system simultaneously. The location of enzymes was directly confirmed by laser scanning confocal microscopy (LSCM) with fluorescent dye labeled lipase. Through comparison experiments with

View Article Online
DOI: 10.1039/C9GC00779B

monophasic and biphasic system, the merits of these two Pickering interfacial catalytic systems, such as high catalysis efficiency, facile products separation and enzymes recycling were intensively demonstrated with esterification of 1-butanol and vinyl acetate. Meanwhile, their underlying principles were preliminarily elaborated. To the best of our knowledge, it is the first report on starch nanoparticles participating in the Pickering emulsion for the recyclable interfacial enzymatic catalysis. The excellent performance makes us believe that this system will attract widespread interest from both fundamental and industrial researchers because it unites some key advantages in terms of green and sustainable chemistry.

Experimental Section

Materials

Native maize starch (MS) was provided by Qin Huangdao LiHua Maize Products Co. (Qin Huangdao, China), the moisture content of starch was 12.2% (w/w), weight-average molecular weight was 2.634×10^7g/mol, number-average molecular weight was 1.29×10^7g/mol. Acetic anhydride (AA), phthalic anhydride (PTA), dimethylsulfoxide (DMSO), N, N-dimethylaminopyridine (DMAP), pyridine, n-heptane were purchased from Aladdin Chemical Reagent Company (Shanghai, China). 1-butanol, vinyl acetate, agarose (Type VII-A, low gelling temperature),

View Article Online
DOI: 10.1039/C9GC00779B

lipase B from *Candida sp.* expressed in *Aspergillus niger* (CALB, liquid form), Tris(hydroxymethyl)aminomethane (Tris) and fluorescein isothiocyanate (FITC) were purchased from Sigma-Aldrich (Shanghai, China).

Preparation of starch amphiphilic nanoparticles

3 g of maize starch was added into 30 mL of DMSO in a 50 mL conical flask. Then the temperature was raised to 40 °C to initiate gelatinization process. After 15 min, the completely gelatinized starch paste was heated to 80 °C followed by the addition of a certain amount of PTA, 10 mL of pyridine and 0.05 g of DMAP, respectively. This esterification reaction was carried out for 3 h under stirring of 200 rpm. After that, a certain amount of AA was added and the mixture was allowed to react for another 3 h at 80 °C under stirring.

The nanosized granulation process was conducted using an water precipitation process. Specifically, 10 mL of composite starch paste was firstly sucked with a disposable syringe (ID 0.3×8 mm). Then, it was added dropwise into the 200mL of water at 1 mL·min^{-1} rate. The resulting suspensions were stirred under 600 rpm for 20 min. Finally, the product was obtained after washing/centrifugation (with water for 3 times) and vacuum drying overnight.

Preparation of Pickering emulsion

View Article Online
DOI: 10.1039/C9GC00779B

Typically, 20 mg of hydrophobic nanoparticles were firstly dispersed in 2 mL of n-heptane under ultrasonication for 10 min, followed by addition of the water phase with the same volume. The resulting mixture was vigorously stirred using an Ultraturrax T25 homogenizer (IKA, Germany) at a stirring rate of 15,000 rpm for 1 min, giving rise to a uniform emulsion composed of a large number of nanoparticle capsules. The formation of Pickering emulsion stabilized by hydrophilic nanoparticles was similar to that of MS-AP (3), except that nanoparticles firstly dispersed in 2 mL of water phase.

Preparation of lipase-loading Pickering emulsion

In a typical experiment, a 40 μL aqueous stock solution of CALB was diluted to 2 mL of Tris-HCl buffered saline (10 mM, pH 7.2) and mixed under shaking for 3 min. This enzyme buffered saline was taken as the water phase, the other procedures followed the same procedures in the preparation of Pickering emulsion as mentioned above.

Assessment of the Catalytic Performance of Lipase

The catalytic performances of CALB were determined via the transesterification of 1-butanol and vinyl acetate in a heptane medium by three different catalytic systems. For Pickering interfacial system, 2 mL of heptane solution containing 150

View Article Online
DOI: 10.1039/C9GC00779B

mmol·L^{-1} 1-butanol and 150 mmol·L^{-1} vinyl acetate was taken as the organic phase to form a lipase-loaded Pickering emulsion. For biphasic system, except for the nanoparticles, the other conditions, including substrate concentration, solvent composition, and lipase content, were the same as given before. For monophasic system, 40 μL aqueous stock solution of CALB was directly added into organic phase with same substrate concentration to initiate the transesterification. All of esterification reactions were carried out with stirring rate of 200 rpm at room temperature. At different time points, A 60 μL aliquot of n-heptane in Pickering interfacial system, biphasic system and monophasic system could be directly extracted. For o/w Pickering interfacial system, after increasing the temperature of system to 40 °C and stirring, the emulsion could be inversed accompanying with organic phase transferring into the upper layer, product could be isolated accordingly. The concentration of the product analyzed via ^{1}H NMR[29]. One unit of lipase activity (U) was defined as 1 μmol of product produced within 1 min. The specific activities (U·μL^{-1}) of lipase were determined under the same condition within 40 min. All reactions were repeated at least three times.

Characterization of starch amphiphilic nanoparticles

The ^{1}H NMR spectra were recorded using an AVANCE digital 400 (Brukev,

View Article Online
DOI: 10.1039/C9GC00779B

Germany) operating at 400 MHz for ^{1}H NMR. The ^{1}H spectra were collected in 128 individual scans with a sweep width of 16 ppm and a delay time of 1 s. Prior to ^{1}H NMR analysis, nanoparticles were dissolved in the deuterium dimethyl sulfoxide (DMSO-d_6) at 40 °C to obtain clear solutions.

Morphology observations were performed using a Merlin scanning electron microscope (Zeiss Co., Germany) at an accelerating voltage of 3 kV. The samples were dispersed in the distilled water (0.05 wt%) under mechanical agitation of 600 rpm for 2 min. One drop of dispersion was carefully placed on a glass slide and dried at room temperature. After that, the samples were coated with Au for conductivity and put under SEM for observations.

The average size of starch nanoparticles was determined through statistical analysis of the geometric parameters including the area, perimeter, diameter which were derived from SEM images using Image-pro Plus 6.0[30].

XRD patterns were obtained using a D/max-IIIA fully automatic XRD instrument (Rigaku, Japan). Diffractograms were collected at 40 kV and 30 mA with nickel-filtered Cu Kα radiation (λ=1.5405 Å). Powdered sample was scanned from 5 to 60°(2θ) at a scanning rate of 4°·min^{-1}. Before XRD analysis, starch nanoparticles were sealed in a vessel at 75% relative humidity using saturated sodium chloride.

View Article Online
DOI: 10.1039/C9GC00779B

Characterization of Pickering Emulsion

The emulsion droplets were visualized using a MB11 polarizing microscope (Shanghai optical instrument factory, China) equipped with a video camera. Emulsion droplets were placed directly onto a glass slide and captured under 50-400 magnification.

The morphology of mircocapsules derived from self-assembly of starch nanoparticles at oil-water interface was measured by SEM. For MS-AP (2) capsules, a few drops of o/w Pickering emulsion were diluted to 10 times with distilled water, then they were added on culture dish and lyophilized. The resulting powders were placed onto a sample stage with an aluminum tape and then coated with Au and put under SEM for observations. For easy characterization of MS-AP (3) capsules, the aqueous core of w/o Pickering emulsion was solidified by addition of agarose (1.5 wt% to the water phase) prior to emulsification. Then the jellified Pickering emulsions were lyophilized and imaged by SEM.

N_2 adsorption/desorption isotherm was measured at 77 K using a Flowsorb Ⅲ 2310 Surface Characterization Analyzer (Micromeritics Instrument Co., USA) after mircocapsules were first degassed at 45 °C overnight. Pore size distribution was determined using the adsorption branch of N_2 isotherms. Mesopore size distribution

View Article Online
DOI: 10.1039/C9GC00779B

was calculated using the Barrett-Joyner-Halenda method (BJH).

Zeta potential measurements of nanoparticles at different pH values were measured using a nano ZS instrument (Malvern Instrument Ltd., UK) equipped with a dip cell. The concentration of nanoparticles was maintained at 0.1 wt % and the experiments were conducted at room temperature.

Water contact angles were measured by analyzing the image of each water droplet on the sample films using a DCa40 MICRO system (DATA physics, Germany). Prior to measurement, the samples were pressed into the films. The films were swollen in the solution at certain pH and then oven-dried at 40 °C for 1 h. Water contact angles were obtained by depositing water droplets of a given pH onto the film that had been previously swollen at the same pH.

To confirm the location of lipase within Pickering emulsion, the lipase molecules were labeled with fluorescein isothiocyanate (FITC) and then were used for formation of Pickering emulsion by following the same procedure as mentioned before. The resulting lipase-loading emulsion were then directly observed with confocal laser scanning microscopy (CLSM, TCS SPE, Leica, America) with an excitation wavelength of 488 nm.

Far-UV circular dichroism (CD) spectra of lipase solutions were measured on a

View Article Online
DOI: 10.1039/C9GC00779B

J-810 CD spectropolarimeter (Jasco Inc., Tokyo, Japan) over a wavelength range of 200-280 nm with a resolution of 0.5 nm. A quartz cell with 1 mm path length was used for CD measurements. Spectra were recorded three times using a scanning speed of 50 nm min^{-1} with a bandwidth of 1.5 nm.

Results and discussion

Synthesis and characterization of starch nanoparticles

The synthesis of starch nanoparticles is illustrated in **Fig.1**. The gelatinization process was firstly performed so as to endow the starch with a high chemical activity by liberalizing the molecular chains to expose more active hydroxyl groups. In this condition, AA and PTA directly participated in the esterification reaction with starch molecules catalyzed by the DMAP and pyridine. Subsequently, the modified starch paste went through the granulation process by water precipitation to obtain the final nanoparticles. Thus, the whole process was performed in an environment that was simple and practical to implement.

It is well established that the interfacial activity of nanoparticles is mainly dictated by their surface characteristics. To screen out an optimal starch nanoparticle, we have prepared a set of samples by adjusting additive amount of AA and PTA. FT-IR spectra of samples are shown in **Fig.2A.** By contrast with MS, the formed

View Article Online
DOI: 10.1039/C9GC00779B

starch products with different substitutions showed the carbonyl antisymmetry deformation vibration at 1751 cm^{-1}, which was a strong ester signal. Besides it increased in intensity with the rise of substitution degree. At the same time, new absorption bands at 1580-1600, 1372, and 1239 cm^{-1} could be assigned to the stretching vibration of benzene rings, symmetrical deformation vibration of methyls and stretch vibration of carbonyls, respectively. The appearance of these new absorptions confirmed the combination of AA and PTA with starch molecules during the esterification process.

^{1}H NMR spectra (**Fig.2B**) gave a clearer composition picture of obtained products. Peaks arising from the anhydroglucose in starch, AA and PTA were assigned according to the literatures[20, 31]. The area of OH-2,3,6 and H-1 protons for anhydroglucose, H-1'proton for AA and H-1'' for PTA are calculated in **Table 1**. On the basis of the method by Chi et al.[31], we estimated the degree of substitution for AA and PTA (DS_{AA} and DS_{PTA}).

From the relatively high values of DS_{AA} in different samples, it suggested that AA as a highly reactive micromolecular agent could steadily graft onto starch chains through esterification. In contrast, due to the steric effects of benzene ring, PTA had a limited reactivity with starch chains by observing its much lower degree of

View Article Online
DOI: 10.1039/C9GC00779B

substitution. Meanwhile, when the additive amount of AA kept constant and PTA increased from 0 to 4.5, a clear decrease was observed for DS_{AA} (2.2 to 0.9). This inferred although AA had a prior reactivity to hydroxyls of anhydroglucose, it still suffered a competition with PTA in the reaction with active sites of starch chains. As a result, it clearly confirmed that chemical composition of starch-based nanoparticles could be easily altered by adjusting additive amount of each ingredient.

In the meantime, the reactive sites were also specified from area of protons (S) in ^{1}H NMR spectra. As expectedly, a decrease was found in the $S_{OH\text{-}2,3}$ of MS-A and MS-P, which meant hydroxyls in C-2 and 3 of anhydroglucose readily participated in the esterification under the employed conditions. In the meantime, the new signals at 4.75, 5.25 and 4.25 ppm corresponding H-2 and H-3 and H-6 signals of anhydroglucose unit in the sugar ester structure are detected. Besides, these signals slightly varied at different of DS_{AA} and DS_{PTA}. However, there was a great discrepancy in the $S_{OH\text{-}6}$ between MS-A and MS-P, in which $S_{OH\text{-}6}$ of MS-A was decreased to 0 whereas $S_{OH\text{-}6}$ of MS-P barely changed. This disclosed the hydroxyls in C-6 were only involved in the AA esterification, showing the hydroxyl heterogeneity of anhydroglucose. The similar phenomenon was also verified by other starch esterification and copolymerzation[32]. Given the above, possible structures of MS-AP

View Article Online
DOI: 10.1039/C9GC00779B

307 are listed in **Fig.1**.

308 In this study, starch nanoparticles were prepared by gelatinization-precipitation
309 process, in which the gelatinization contributed to the regularity destruction of native
310 starch granules. Therefore, the obtained products were mainly in amorphous forms, as
311 proved by mostly diffuse peaks in the corresponding XRD diffraction spectrum
312 (**Fig.S1**). Furthermore, since the change of composition directly affected the
313 molecular weight, polarity, and charge, etc. of dissolved polymer, there would be
314 differences in the granulation process for different samples in terms of formation of
315 aggregations in the supersaturation region and subsequent particle growth process
316 within a poor solvent[33]. From **Figure.3A**, nano-granulation of native starch could not
317 be achieved by only finding a block of deformed sedimentations in MS. This was
318 because hydroxyl-rich unmodified starch chains (water contact angle of 41° for MS)
319 possessed a similar polarity to water, which had a difficulty in entangling with each
320 other in the solvent conversion from DMSO to water. In stark contrast, MS-A
321 exhibited a regular spherical nanoparticle with average size of 421nm (**Figure.3B** and
322 **Figure S2**). We attributed this improvement to the "bridging action" brought by
323 introduced acetyls. Since the carbonyls could form hydrogen bonds with hydroxyls[24],
324 acetyls played a role of "bridge" that facilitated to connect other starch chains, thus

View Article Online
DOI: 10.1039/C9GC00779B

more cross-linking occurred between modified starch chains in DMSO. In this condition, exposed methyls played an important role in generating a hydrophobic surface (water contact angle of 112° for MS-A), which not only facilitated the formation of aggregations during the solvent conversion, but also avoided the collapse and adhesion of obtained nanoparticles in particle growth process.

Moreover, when PTA was introduced to the synthesis of starch nanoparticles, residual carboxyls of phthalic ester were of great importance in adjusting the charge of modified starch chains. From zeta potential of MS-APs (**Table.S1**), it was clear that dissociated carboxyls increased the negative charge of modified starch chains in employed condition. This enhanced electrostatic repulsion between modified starch chains possibly induced more localized aggregations formed by a smaller number of modified starch chains in the supersaturation region, thus resulting in a limited size of formed particles (**Figure.3C-E**). With rational DS_{AA} and DS_{PTA}, amphipathic MS-AP (2) and (3) achieved ideal wettablities (water contact angle near to 90°) and presented regular spheres with average size of 197 and 185nm, respectively. However, for MS-AP (1), higher DS_{PTA} induced more hydrophilicity of surface, thus particles adhered to each other to form clusters in the end. With only PTA grafting onto starch chains, MS-P (**Figure.3F)** exhibited highest zeta potential (-26.93mV) and lowest

View Article Online
DOI: 10.1039/C9GC00779B

water contact angle (13°). As expectedly, MS-P was still in the form of starch paste due to the increased electrostatic repulsion and excessive hydrophilicity.

Characterization of o/w and w/o Pickering emulsions

Before the formation of emulsion, we firstly observed the dispersibility of these samples with different chemical characteristics in water/n-heptane solution. As shown in **Fig.4**, hydroxyl-rich MS only dispersed in the aqueous phase, while MS-A after hydrophobic modification dispersed well in n-heptane. For MS-AP (3), they initially dispersed in organic phase, but transferred to the n-heptane-water interface within 10 min, suggesting their excellent amphiphilicity. Interestingly, a completely opposite phenomenon was observed for MS-AP (2), where nanoparticles firstly dispersed well in aqueous phase and subsequently transferred to the interface. When it came to MS-AP (1) and MS-P, both samples steadily dispersed in the aqueous phase. However, it was worth noting that dispersion of MS-P in the aqueous phase exhibited more transparent because starch was mainly present in the form of dissolved molecular chain.

Subsequently, we applied these samples to form Pickering emulsion and then investigated the status of the emulsion. In specific experiment, based on the surface characteristics, 1 wt% of sample was firstly dispersed in n-heptane or water, followed

View Article Online
DOI: 10.1039/C9GC00779B

by addition of the other phase with the same volume. After homogenization (12000 rpm, 60 s), the resulting emulsion was allowed to stand at room temperature for 10 min without any disturbance. The emulsion type was determined by the conductivity analysis. As shown in **Fig.5**, a demulsification was observed as soon as the emulsion was formed in the emulsions stabilized by MS, MS-AP (1) and MS-P, which confirmed these samples were unable to stabilize the emulsion mainly due to their deformed morphology, non-uniform size and high hydrophilicity. Furthermore, the use of hydrophobic MS-A as stabilizers led to the formation of w/o emulsion, but it had low stability, as evidenced by the obvious increase in droplet size after standing for 10 min. Noteworthily, because of regular morphology and excellent amphiphilicity, MS-AP (2) and MS-AP (3) both had better emulsifying capacities, leading to the long-lasting stable emulsion layers. The only difference was that, for MS-AP (3) stabilized w/o Pickering emulsion, since the emulsion droplets with water core possessed a higher density compared to continuous phase n-heptane, the emulsion layer would sink to the bottom. In contrast, because of oil core, droplets in o/w Pickering emulsion stabilized by MS-AP (2) possessed a lower density compared to continuous phase water, the emulsion layer would float on the top.

Fig. 6A, D shows microscopic images of the droplets acquired from the emulsion

View Article Online
DOI: 10.1039/C9GC00779B

379 stabilized by MS-AP (3) and MS-AP (2). The results indicated that both droplets had
380 a similar diameter range of 5-30 μm, which was related to the similar size of
381 stabilizers. However, in contrast to MS-AP (2) stabilized o/w emulsion that possessed
382 a uniform distribution of intact droplets, MS-AP (3) stabilized w/o emulsion had an
383 unsatisfactory status, in which the macroscopic agglomerations of stabilizers were
384 dispersed in the continuous phase and adhered to the surface of droplets. Scanning
385 electron microscopy (SEM) imaging confirmed this discrepancy. It clearly revealed
386 that the droplets of o/w Pickering emulsion stabilized by MS-AP (2) were regular
387 spheres (**Fig.6E, F**). The shell of the intact sphere was firm and remained unbroken
388 even in the freeze-drying process. After the formed spheres were greatly grinded with
389 a mortar, the broken spheres revealed the hollow interior, confirming the
390 microcapsule structures (**Fig.6J, K**). Moreover, their shells were thin and consisted of
391 one or two layers of starch-based nanoparticles (**Fig.6L**). In contrast, although most
392 droplets in Pickering emulsion stabilized by MS-AP (3) presented intact hollow
393 capsules as well (**Fig.6B, C, G, H**), excessive particles adhering to the surface greatly
394 increased the thickness of the shell (**Fig.6I**). This phenomenon was mainly due to the
395 discrepancy in dispersibility of starch nanoparticles in different solvent. In this study,
396 hydrophilic MS-AP (2) easily achieved regular arrangement when immersed in the

View Article Online
DOI: 10.1039/C9GC00779B

397 water phase. The rational electrostatic repulsion brought by surface charges ensured
398 the stabilization of MS-AP (2) dispersion. Its corresponding polydispersity index (PDI)
399 was 0.125 (calculated by size distribution), which suggested the monodispersity of
400 particles. In contrast, although MS-AP (3) had a better wettability to organic phase
401 with higher DS_{AA}, the residual hydroxyls and carboxyls made inevitable repulsions
402 with n-heptane molecules, which induced MS-AP (3) to form the agglomeration in
403 organic phase. Because of this, there were easy particle sedimentations on the surface
404 of droplets in the formation of Pickering emulsion. The similar phenomenon was also
405 found in our previous report[34].

406 **Biocatalytic performances of Pickering interfacial catalytic systems**

407 For construction of interfacial enzymatic catalytic system, we introduced CALB
408 as the target enzyme. Then Tris-HCl buffered saline (10 mM, pH 7.2) with CALB
409 was taken as the water phase of Pickering emulsion. Since the continuous phase and
410 dispersed phase were reversed for Pickering emulsion stabilized by MS-AP (2) and
411 MS-AP (3), CALB should be distributed inside and outside the shell of capsules,
412 respectively. To confirm this assumption, CALB molecules were firstly labeled with
413 FITC and then used for the formation of Pickering emulsion by following the same
414 procedure as mentioned before. As shown in **Fig.7A, B**, CLSM imaging clearly

View Article Online
DOI: 10.1039/C9GC00779B

415 revealed that the emulsion stabilized by MS-AP (3) was composed of green capsules
416 and thus indicated that the interior of capsules was loaded with FITC-labeled lipase
417 molecules. But for MS-AP (2), the green fluorescent was observed around the blank
418 capsules, which confirmed the lipase molecules dispersed outside the capsules
419 (**Fig.7C, D**). **Fig.7E, F** illustrated the forming process of these two interfacial
420 enzymatic catalytic systems.

421 Furthermore, to determine whether the lipase was destroyed during the
422 emulsification process, we used CD spectra to identify the secondary structure of the
423 free lipase before emulsification and after release from the Pickering emulsions via
424 centrifugation (10000rpm, 5min). As shown in **Fig.S3**, the CD spectra showed little
425 changes in terms of secondary structure, suggesting that the emulsification process
426 insignificantly impacted the enzyme.

427 The biocatalytic performances of these two CALB loaded Pickering interfacial
428 catalytic systems were then investigated by transesterification of 1-butanol and vinyl
429 acetate. To confirm their superiorities, two other catalytic systems, biphasic and
430 monophasic enzymatic reactions containing same amount of free CALB, were carried
431 out as negative controls. As shown in **Fig.8A**, the conversion rate of the reaction in
432 o/w Pickering interfacial catalytic system reached 100% within 8 h. In the meantime,

View Article Online
DOI: 10.1039/C9GC00779B

92% conversion was observed for w/o Pickering interfacial catalytic system. In stark contrast, a significant reaction inhibition was observed for biphasic and monophasic catalytic system, where only 60% and 32% conversion rate were achieved at the same time. For directly comparing the catalytic activity of enzyme, the specific activity of CALB for each system was calculated according to the conversion rate obtained within 40 min. As shown in **Fig.8B**, free lipase dissolved in n-heptane only had a specific activity of 0.0198U·μL^{-1}, which clearly indicated that long-term exposure of free enzymes to an organic solvent caused reduced enzyme activity. Comparatively, the increased specific activity (0.0282U·μL^{-1}) in the water/n-heptane biphasic system suggested that enzymes typically preferred an aqueous environment, which protected them effectively from the organic media. However, inefficient mass transfer between two phases resulted in the low conversion rate even after a long reaction time. Delightfully, the formation of Pickering emulsion significantly improved the catalytic activity of CALB by observing higher specific activities of 0.0724U·μL^{-1} and 0.0843U·μL^{-1} for w/o and o/w Pickering interfacial catalytic system, respectively. In accordance with previous report, the higher catalytic activity could be attributed to the nanoparticles-assembled capsules, which not only functioned as an idea screen for preserving enzyme activity in organic solvent, but also provided increased interfacial

View Article Online
DOI: 10.1039/C9GC00779B

areas that improved mass transfer and accessibility of enzyme molecules. More importantly, by comparing specific activities of CALB between o/w and w/o Pickering interfacial catalytic system, we proposed that the location of two phases in Pickering emulsion also played a key role in the catalytic capacity.

To give a deeper insight of this proposal, the whole reaction processes for transesterification of 1-butanol and vinyl acetate in o/w and w/o Pickering interfacial catalytic system are illustrated in **Fig.9.** Given the same phases (water and organic phases) and elements (substrates, enzymes and stabilizers), the reaction processes in both two systems mainly composed of five steps: (1) enzymes dissolved in the water phase and substrates dissolved in the organic phase transferred to the emulsion droplet surface simultaneously, (2) enzymes and substrates both accessed to the n-heptane-water interface, (3) the catalytic reaction took place on the interface, (4) after the end of reaction, products and enzymes departed from the interface, (5) products entered the organic phase and enzymes entered the water phase, respectively. Clearly, step (1) and (5) mainly involved mass transfer in the phase, whereas step (2) and (4) were closely related to the mass transfer on the interface.

As described in **Fig.9A**, the continuous phase of the o/w Pickering emulsion served as an avenue for enzyme transfer. Because of good water solubility, enzymes

View Article Online
DOI: 10.1039/C9GC00779B

could be uniformly distributed around the droplets in the water phase. Densely dispersed oil droplets as microreactors efficiently confined substrates in tight spaces. The resulting decreased transfer distance in organic phase was beneficial for substrates to contact with enzymes distributed on the interface and thus resulted in a higher specific activity. In stark contrast, the continuous phase of the w/o Pickering emulsion was n-heptane (**Fig.9B**), so that it served as an avenue for substrates transport. Given that enzymes were uniformly distributed within the droplets, thus enzymatic reaction was determined by the transfer of substrates in bulk continuous phase. Since transfer distance outside droplets was much larger, it was reasonable that specific activity of CALB in w/o Pickering emulsion was relatively low.

In view of increasing stirring rate could enhance the mass transfer in the phase, we compared the catalysis efficiency of these two systems under different stirring input powers in **Fig.10A** (a larger stirring input power corresponds to a higher stirring rate; the relationships were reflected in **Table.S2**). For MS-AP (2) stabilized o/w Pickering interfacial catalytic system, specific activity of CALB slightly increased with increasing stirring input power and then leveled off after the stirring input power exceeded 12.5 W. The maximum specific activity for transesterification reached 0.0868U·μL^{-1}, which was only 4.8% higher than original value. This limited increase

View Article Online
DOI: 10.1039/C9GC00779B

clearly confirmed a higher stirring rate had little impact on the catalysis efficiency of o/w Pickering interfacial catalytic system, which was due to the short transfer distance of substrates brought by droplets that had already promoted the interfacial reaction as much as possible. When it came to MS-AP (3) stabilized w/o Pickering interfacial catalytic system, specific activity of CALB underwent a sharp increase with increasing stirring input power. Notably, its maximum catalysis efficiency could reach $0.0853 U \cdot \mu L^{-1}$ after the stirring input power exceeding 22.5 W, which was close to o/w emulsion system. As expectedly, elevating stirring input power was more effective in improving the catalysis efficiency of w/o Pickering interfacial catalytic system by accelerating the transfer of substrates in bulk continuous phase. The similar results were also reported by Huo[35] in the Pt-catalyzed interfacial reaction.

As mentioned above, the shell of hollow microcapsules was composed by the layers of starch nanoparticles, whose status was closely related to the mass transfer on the interface. For the o/w Pickering emulsion stabilized by MS-AP (2), self-assembled starch nanoparticles at the n-heptane-water interface yielded a stable shell with one or two nanoparticle thickness. Pore-size-distribution curves were plotted based on the nitrogen adsorption-desorption isotherms using the BJH method (**Fig.S4**). The result revealed microcapsules formed by MS-AP (2) had a board pore distribution ranging

View Article Online
DOI: 10.1039/C9GC00779B

505 from 3 nm to 120nm. (**Fig.10B**). This confirmed that, in contrast to the uniform
506 distribution of inorganic particles at the oil-water interface, the starch nanoparticles
507 presented an irregular arrangement. Pores with size of less than 10 nm likely arose
508 from the interspaces between the starch nanoparticles closely arranged at the oil-water
509 interface. In the meantime, pores with larger size were mainly due to the gaps
510 between the layers of starch nanoparticles. As the hydrate diameters of the substrate
511 and the product molecules were about 0.6–0.8 nm (calculated by Material Studio
512 software, **Fig.S5**) and CALB had dimensions of 3×4×5 nm[36], it could be deduced that
513 the shell of the microcapsules could allow the free diffusion of enzymes, substrates
514 and products. When it came to microcapsules formed by MS-AP (3), the data showed
515 an increase in the pore size of 5~10 nm whereas decrease in the pore size of 10~100
516 nm. This result indicated that excessive adhesion of starch nanoparticles to the surface
517 of droplets brought about more serious agglomeration, which resulted in not only
518 closer arrangement between MS-AP (3) at the oil-water interface, but also more
519 compressed space in the multilayer of starch nanoparticles(**Fig.10B**).

520 To quantificationally clarify the discrepancy in mass transfer on the interface
521 between these two systems, we designed a pure Pickering emulsion by tripling the
522 concentration of nanoparticles prior to emulsification (**Fig.11**), in which the emulsion

View Article Online
DOI: 10.1039/C9GC00779B

layer would not sink to the bottom or float on the top. In this condition, droplets with dense and uniform distribution in the w/o Pickering emulsion confined the majority of mass transfer to the local interfacial area instead of bulk continuous phase. Meanwhile, decreased size of droplets in the o/w Pickering emulsion also contributed to more mass transfer on the interface, as similar as possible to the situation in w/o Pickering emulsion. Subsequently, we determined the enzymatic Michaelis-Menten kinetics of CALB with respect to substrates between these two systems (**Fig.S6**). It was found that the CALB in o/w emulsion showed K_m value of 464 mM and v_{max} value of 17.54 $mM \cdot min^{-1}$, whereas the K_m and v_{max} of CALB in w/o emulsion was 547 mM and 8.77 $mM \cdot min^{-1}$, respectively. A lower K_m and higher v_{max} indeed confirmed o/w emulsion exhibited a higher affinity of CALB toward substrates on the interface, which agreed well with its shell structure with favorable mass transfer channels.

Finally, the apparent activation energy estimation was used to analyze the mass transfer resistance of both systems[37]. **Fig.S7A, B** shows the kinetics plots of transesterification in these two systems at different reaction temperatures. Clearly, the w/o Pickering interfacial catalytic system was more temperature sensitive than that of the o/w Pickering interfacial catalytic system. Based on these kinetics plots, we could estimate the apparent reaction rate constants of these two systems. As shown in

View Article Online
DOI: 10.1039/C9GC00779B

Fig.S7C, plots of ln k versus 1/T for the transesterification in these two systems were both linear over the investigated temperature range, which suggested that the temperature effects on the apparent reaction rate constant followed the Arrhenius equation. Based on the Arrhenius equation, the apparent activation energies of the o/w and w/o Pickering interfacial catalytic system were estimated to be 19.8 and 26.9 $kJ \cdot mol^{-1}$, respectively. These results confirmed that the o/w Pickering interfacial catalytic system had a lower mass transfer resistance in comparison with w/o system.

Recycling and Applicability

Benefiting from organic phase located outside the shell of capsule, MS-AP (3) stabilized w/o Pickering interfacial catalytic system allowed us to effectively recycle the reaction (**Fig.12A**). At the end of each reaction cycle, the emulsion layer and excess organic phase were automatically separated into two layers with a clear boundary. When organic phase was removed through a simple decantation, the residual emulsion layer could be directly used in the next batch. After adding fresh n-heptane, a new interfacial enzymatic system was formed without the need for further emulsification. The emulsion droplet morphology and size were maintained during the course of consecutive reaction cycles (**Fig.S8**). To our delight, this MS-AP (3) stabilized w/o Pickering interfacial catalytic system was highly recyclable, which

View Article Online
DOI: 10.1039/C9GC00779B

559 was highlighted by least 10 reaction cycles (**Fig.12B**). Given that the secondary
560 structure of enzyme has been proved to be intact in the emulsion layer, the slight
561 reduction of conversion rate was mainly due to enzyme leakage during the mixing of
562 two phases. Although the yields of the first reaction cycle was about 60.7%, from the
563 second reaction cycle onward the yields increased up to 93–99%. This high
564 conversion and significantly simplified process justified the effectiveness of MS-AP
565 (3) stabilized w/o Pickering interfacial catalytic system in product separation and
566 enzyme recycling.

567 However, the recycling of reaction was not easy to achieve in the MS-AP (2)
568 stabilized o/w Pickering interfacial catalytic system. It is well documented that
569 particle-stabilized emulsion has extremely high stability because a high energy barrier
570 confines the nanoparticles at the interface of droplets. As a result, organic phase
571 within the capsules could not be separated out easily. Inspired by Yang[38], the
572 emulsion-inversion might provide a feasible way of transferring organic phase
573 because it was not accompanied with detachment of solid particles from the oil-water
574 interface. Given the pH-responsive surface characteristics of MS-AP (2) brought by
575 phthalic ester, we attempted to achieve the emulsion-inversion by adjusting the pH of
576 system. However, it was worth mentioning that frequent pH adjustment by directly

View Article Online
DOI: 10.1039/C9GC00779B

adding acids and bases was not an ideal process for recycling enzymatic catalysis. This was because it took much more acids and bases to break the buffer system prior to changing pH, the resulting excessive salts inevitably deteriorated the pH-responsiveness of emulsion[34]. Moreover, enzyme activity was vulnerable to the environment due to the lack of buffer protection.

Since the pH of Tris-HCl buffer was temperature-responsive[39, 40], it reminded us to control the pH of MS-AP (2) stabilized o/w Pickering interfacial catalytic system by adjusting temperature. Impressively, when the temperature of system was elevated to 45°C, the corresponding pH of water phase was decreased to 6.4 (no damage to the structure of the enzyme, **Fig.S9**). After emulsification process, MS-AP (2) transferred to the bottom layer to form w/o emulsion. More interestingly, if cooling the system to room temperature, the pH was back to 7.2, accordingly. Then MS-AP (2) again transferred back to the upper layer to form o/w emulsion after emulsification (**Fig.13A**). Therefore, a facile recyclable procedure for MS-AP (2) stabilized o/w Pickering emulsion was achieved: (1) lowered pH at high temperature to induce w/o emulsion, organic phase with products was removed. (2) supplemented the fresh organic phase and elevated pH by decreasing temperature to regain o/w emulsion for recycling the reaction (**Fig.13B**). However, the repeated use of the emulsification

View Article Online
DOI: 10.1039/C9GC00779B

process for recycling reaction would induce more serious phase lost, capsule breakage and deformation (**Fig.S10**). Therefore, a less yield and conversion rate were obtained in each cycle of o/w Pickering emulsion in comparison to w/o Pickering emulsion (**Fig.13C**).

For clarifying the role of MS-AP (2) in the regulation of emulsion-inversion, its surface characteristics were analyzed at different pH. As shown in **Fig.13D**, under the weak acid conditions (pH 6.4), the zeta potential of MS-AP (2) was measured to be -13.4 mV. As the pH value slightly increased, the zeta potential increased owing to the gradual deprotonation of carboxyls. When pH value reached 10, the zeta potential became -22.1 mV, suggesting a nearly full deprotonation of the carboxyls. The carboxyls deprotonation at the high pH values made the nanoparticles surface hydrophilic owing to it bearing charges, whereas the protonation of carboxyls at low pH values rendered the surface hydrophobic[38], which endowed MS-AP(2) with a better wettabity to organic phase. This pH-triggered hydrophilicity/hydrophobicity switching was confirmed by water contact angle measurements (**Fig.13D**). The water contact angle of fresh MS-AP (2) (point a) was 84°, whereas the water contact angle of MS-AP (2) treated with an acidic aqueous solution (pH 6.4, point b) increased to 92°. When the protonated MS-AP (2) was further treated with a basic solution (pH 7.8,

View Article Online
DOI: 10.1039/C9GC00779B

point c), its water contact angle restored the value (82°).

Furthermore, to check the applicability of these two systems, we conducted transesterification of other substrates with a regular carbon chain growth. **Table.2** lists the results of transesterification in the first and second reaction cycles. For substrates with shorter carbon chains($C \leqslant 8$), the o/w and w/o Pickering interfacial catalytic system were both effective in the transesterification, achieving 100% conversion rate within 20 h. At the end of the first reaction cycle, the yields of 57-65% was directly obtained through simple phase separation. The yields increased up to 88-96% from the second reaction cycle onwards. For substrates with longer carbon chains($C>8$), substrate concentration was reduced to 60 mmol/L to ensure complete solubility in the reaction solvent. In this condition, 83-90% conversion rate was achieved in the o/w Pickering interfacial catalytic system, whereas 76-82% conversion rate in w/o system. These results suggested that the both two systems had a high flexibility in tolerating various substrates.

Conclusion

In summary, we have prepared amphiphilic starch nanoparticles by the grafting of AA and PTA onto maize starch, followed by the gelatinization-precipitation process. Then they were employed to construct Pickering interfacial catalytic system

View Article Online
DOI: 10.1039/C9GC00779B

for enhancing enzyme activity in organic solvent. Due to the distinct surface characteristics of MS-AP (2) and MS-AP (3), we succeeded to design o/w and w/o Pickering interfacial catalytic system at the same time. When CALB was chosen as a model enzyme and esterification of 1-butanol and vinyl acetate as catalytic reaction, these two Pickering interfacial catalytic systems both exhibited significantly enhanced catalysis efficiency in comparison with monophasic and biphasic system. By contrast, a higher catalysis efficiency was achieved in o/w Pickering interfacial catalytic system because of less substrate transfer distance in phase and higher enzyme affinity on the interface. Impressively, the products could be isolated from both Pickering interfacial catalytic systems and their high effectiveness was highlighted by at least 10 reaction cycles. By this successive products separation and enzymes recycling system, the overall efficiency of an enzymatic process might be significantly improved and the work-up method might be simplified. The amphiphilic starch nanoparticles that participate in the facile construction of recycling Pickering interfacial enzymatic catalysis will attract widespread interest because it is in accordance with the concept of green and sustainable chemistry.

Acknowledgements

This research was supported by the National Natural Science Foundation of Chin

View Article Online
DOI: 10.1039/C9GC00779B

a (21878106 and 21576098), Fundamental Research Funds for the Central Universities, SCUT (2018ZK08), National International Science and Technology Cooperation Base for Tropical Health Food (2017D01005), 111 Project (B17018), the Key Project of Science and Technology of Guangdong Province (2018A050506016,2017B090901002).

Reference

1. R. A. Sheldon and S. van Pelt, *Chemical Society reviews*, 2013, **42**, 6223-6235.
2. M. Hartmann and X. Kostrov, *Chemical Society reviews*, 2013, **42**, 6277-6289.
3. J. Liu, G. Lan, J. Peng, Y. Li, C. Li and Q. Yang, *Chemical communications*, 2013, **49**, 9558-9560.
4. Z. Wang, M. C. van Oers, F. P. Rutjes and J. C. van Hest, *Angewandte Chemie*, 2012, **51**, 10746-10750.
5. Z. Sun, U. Glebe, H. Charan, A. Böker and C. Wu, *Angewandte Chemie*, 2018, **130**, 14006-14010.
6. X. Yang, Y. Wang, R. Bai, H. Ma, W. Wang, H. Sun, Y. Dong, F. Qu, Q. Tang and B. Binks, *Green Chemistry*, 2019.
7. F. Rudroff, M. D. Mihovilovic, H. Gröger, R. Snajdrova, H. Iding and U. T. Bornscheuer, *Nature Catalysis*, 2018, **1**, 12.
8. Z. Chen, L. Zhou, W. Bing, Z. Zhang, Z. Li, J. Ren and X. Qu, *Journal of the American Chemical Society*, 2014, **136**, 7498-7504.
9. J. Shi, X. Wang, W. Zhang, Z. Jiang, Y. Liang, Y. Zhu and C. Zhang, *Advanced Functional Materials*, 2013, **23**, 1450-1458.
10. L.-H. Xue, C.-Y. Xie, S.-X. Meng, R.-X. Bai, X. Yang, Y. Wang, S. Wang, B. P. Binks, T. Guo and T. Meng, *ACS Macro Letters*, 2017, **6**, 679-683.
11. F. Cuomo, A. Ceglie, A. De Leonardis and F. Lopez, *Catalysts*, 2019, **9**, 1.
12. Y. Chen, Z. Li, H. Wang, Y. Pei, Y. Shi and J. Wang, *Langmuir : the ACS journal of surfaces and colloids*, 2018, **34**, 2784-2790.
13. L. Peng, A. Feng, S. Liu, M. Huo, T. Fang, K. Wang, Y. Wei, X. Wang and J. Yuan, *ACS applied materials & interfaces*, 2016, **8**, 29203-29207.

14. B. Binks and S. Lumsdon, *Langmuir : the ACS journal of surfaces and colloids*, 2001, **17**, 4540-4547.
15. Z. Zhai, Q. Wu, J. Li, B. Zhou, J. Shen, Z. H. Farooqi and W. Wu, *Journal of Catalysis*, 2019, **369**, 462-468.
16. Z. Fang, D. Yang, Y. Gao and H. Li, *Colloid and Polymer Science*, 2015, **293**, 1505-1513.
17. W.-J. Zhou, L. Fang, Z. Fan, B. n. Albela, L. Bonneviot, F. De Campo, M. Pera-Titus and J.-M. Clacens, *Journal of the American Chemical Society*, 2014, **136**, 4869-4872.
18. J. Tang, P. J. Quinlan and K. C. Tam, *Soft matter*, 2015, **11**, 3512-3529.
19. C. Cai, B. Wei, Z. Jin and Y. Tian, *Acs Sustainable Chemistry & Engineering*, 2017, **5**.
20. Y. Tan, K. Xu, C. Liu, Y. Li, C. Lu and P. Wang, *Carbohydrate Polymers*, 2012, **88**, 1358-1363.
21. S. B. Haaj, W. Thielemans, A. Magnin and S. Boufi, *Acs Applied Materials & Interfaces*, 2014, **6**, 8263.
22. Y. Habibi and A. Dufresne, *Biomacromolecules*, 2008, **9**, 1974-1980.
23. H. Namazi and A. Dadkhah, *Carbohydrate Polymers*, 2010, **79**, 731-737.
24. Y. Xu, W. Ding, J. Liu, Y. Li, J. F. Kennedy, Q. Gu and S. Shao, *Carbohydrate Polymers*, 2010, **80**, 1078-1084.
25. M. Jonoobi, J. Harun, A. P. Mathew, M. Z. B. Hussein and K. Oksman, *Cellulose*, 2010, **17**, 299-307.
26. T. M. Don, S. C. Chou, L. P. Cheng and H. Y. Tai, *Journal of Applied Polymer Science*, 2011, **120**, 1-12.
27. Y. Tan, K. Xu, L. Li, C. Liu, C. Song and P. Wang, *ACS applied materials & interfaces*, 2009, **1**, 956-959.
28. S. F. Chin, S. C. Pang and S. H. Tay, *Carbohydrate Polymers*, 2011, **86**, 1817-1819.
29. J. Huo, J. Aguilera-Sigalat, S. El-Hankari and D. Bradshaw, *Chemical science*, 2015, **6**, 1938-1943.
30. L. Qi, J.-H. Cheng, X.-Y. Liang and Y.-Y. Hu, *Polymer Engineering & Science*, 2016, **56**, 158-169.
31. H. Chi, K. Xu, X. Wu, Q. Chen, D. Xue, C. Song, W. Zhang and P. Wang, *Food chemistry*, 2008, **106**, 923-928.
32. H. Chi, K. Xu, D. Xue, C. Song, W. Zhang and P. Wang, *Food research international*, 2007, **40**, 232-238.
33. D. Quintanar-Guerrero, E. Allémann, E. Doelker and H. Fessi, *Colloid and Polymer Science*, 1997, **275**, 640-647.
34. L. Qi, Z. Luo and X. Lu, *Green Chemistry*, 2018, **20**, 1538-1550.

35. J. Huo, M. Marcello, A. Garai and D. Bradshaw, *Adv Mater*, 2013, **25**, 2717-2722.
36. M. Foresti, G. Valle, R. Bonetto, M. Ferreira and L. Briand, *Applied Surface Science*, 2010, **256**, 1624-1635.
37. H. Liu, Z. Zhang, H. Yang, F. Cheng and Z. Du, *ChemSusChem*, 2014, **7**, 1888-1900.
38. H. Yang, T. Zhou and W. Zhang, *Angewandte Chemie*, 2013, **52**, 7455-7459.
39. D. Perrin, *Buffers for pH and metal ion control*, Springer Science & Business Media, 2012.
40. R. A. Durst and B. R. Staples, *Clinical Chemistry*, 1972, **18**, 206-208.

View Article Online
DOI: 10.1039/C9GC00779B

722 **Table.1** Results of ^{1}H NMR spectrum and calculated degree of substitution for starch products

723 with various compositions.

Sample	Additive amount: MS (g)/ AA(g)/ PTA (g)	Area of protons(S) 5.40-5.50ppm (OH-2,3)	4.59ppm (OH-6)	5.10ppm (H-1) [a]	2.02ppm (H-1')	7.65ppm (H-1'')	DS_{AA}	DS_{PTA}
MS	3/0/0	2.04	1.01	1.00	-	-	-	-
MS-P	3/0/4.5	1.89	0.99	1.00	-	0.22	-	0.15
MS-AP(1)	3/4.5/4.5	1.55	0.31	1.00	2.51	0.14	0.90	0.07
MS-AP(2)	3/4.5/2.25	1.09	-	1.00	4.67	0.08	1.70	0.04
MS-AP(3)	3/4.5/1.5	0.78	-	1.00	5.81	0.03	2.08	0.02
MS-A	3/4.5/0	0.71	-	1.00	6.30	-	2.20	-

724 [a] Area of H-1 protons was set as the basic value 1.

View Article Online
DOI: 10.1039/C9GC00779B

Table.2 Results for the first and second reaction cycles of the transesterification of various substrates in the o/w and w/o Pickering interfacial catalytic system..

Substrates	Substrates concentration ($mmol \cdot L^{-1}$)	t (h)	o/w Pickering emulsion				w/o Pickering emulsion			
			Run 1		Run 2		Run 1		Run 2	
			Y (%)[a]	C[a] (%)	Y (%)	C (%)	Y (%)	C (%)	Y (%)	C (%)
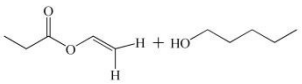	150	20	57.3	100	91.2	100	63.2	100	95.5	100
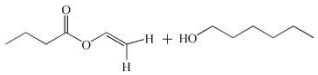	150	20	58.5	100	88.2	100	64.7	100	94.2	100
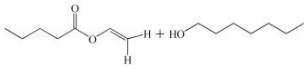	150	20	58.3	100	93.1	100	65.3	100	94.1	100
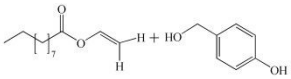	60	20	57.2	92.3	92.4	91.4	66.1	83.7	93.2	81.7
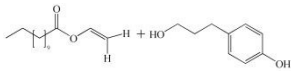	60	20	58.1	88.1	91.6	89.7	65.4	81.4	94.1	80.3
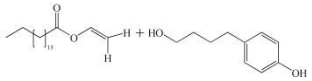	60	20	59.1	83.1	89.3	84.2	65.6	76.2	93.4	77.8

[a] Y and C stands for yield and conversion rate, respectively.

View Article Online
DOI: 10.1039/C9GC00779B

Figure Caption

Figure.1 Schematic representation of possible mechanisms for preparation of starch nanoparticles.

Figure.2 FT-IR (A) and ^{1}H NMR (B) spectra of starch products after gelatinization-esterification-precipitation process. Designation “a” and ‘‘b” refer to signals attributed to protons of anhydroglucose unit before and after esterification, respectively.

Figure.3 SEM images and water contact angles of (A) MS, (B) MS-A, (C) MS-AP (3), (D) MS-AP (2), (E) MS-AP (1) and (F) MS-P and their responding forming mechanism diagrams. Scale bar: 1μm.

Figure.4 Suspension of starch products in water/n-heptane solution.

Figure.5 Status of the Pickering emulsion stabilized by various starch products.

Figure.6 Optical micrograph of droplets in Pickering emulsion stabilized by (A) MS-AP (3) and (D) MS-AP (2). SEM images of microcapsules formed by the self-assembly of (B, C) MS-AP (3) and (E, F) MS-AP (2). SEM images of broken microcapsules formed by (G, H) MS-AP (3) and (J, K) MS-AP (2). SEM images of the cross section of layer in microcapsules formed by (I) MS-AP (3) and (L) MS-AP (2).

Figure.7 (A, B) CLSM images of the MS-AP (3) self-assembled capsules containing FITC-labeled lipase. (C, D) CLSM images of MS-AP (2) self-assembled capsules surrounded by FITC-labeled lipase (scale bar for (A) and (C) is 50μm, for (B) and (D) is 10μm). (E, F) Forming process of two interfacial enzymatic catalytic systems.

Figure.8 (A) Time dependent conversion rate of butyl acetate catalyzed by different biocatalytic system. (B) Specific activity of CALB for each biocatalytic system.

Figure.9 Reaction processes for transesterification in (A) o/w and (B) w/o Pickering interfacial catalytic system.

Figure.10 (A) Specific activities of CALB for the o/w and w/o Pickering interfacial catalytic system under different stirring input powers. (B) Mesopore-size distributions of microcapsules shell formed by MS-AP (2) and MS-AP (3), calculated by the BJH absorption method.

Figure.11 Reaction processes for transesterification in (A) o/w and (B) w/o pure Pickering interfacial catalytic system.

Figure.12 (A) Recycling process of w/o Pickering interfacial catalytic system. (B) Recycling results for the transesterification in the w/o Pickering interfacial catalytic system, reaction time was 20 h.

Figure.13 (A) Photographs of successive temperature-responsive MS-AP (2) stabilized o/w Pickering emulsion (1st, 2nd, 5th and 10th cycle). (B) Recycling process of o/w Pickering interfacial catalytic system. (C) Recycling results for the transesterification in the o/w Pickering interfacial catalytic system, reaction time was 12h. (D) Zeta potentials and water contact angles of MS-AP (2) treated with different pH value.

View Article Online
DOI: 10.1039/C9GC00779B

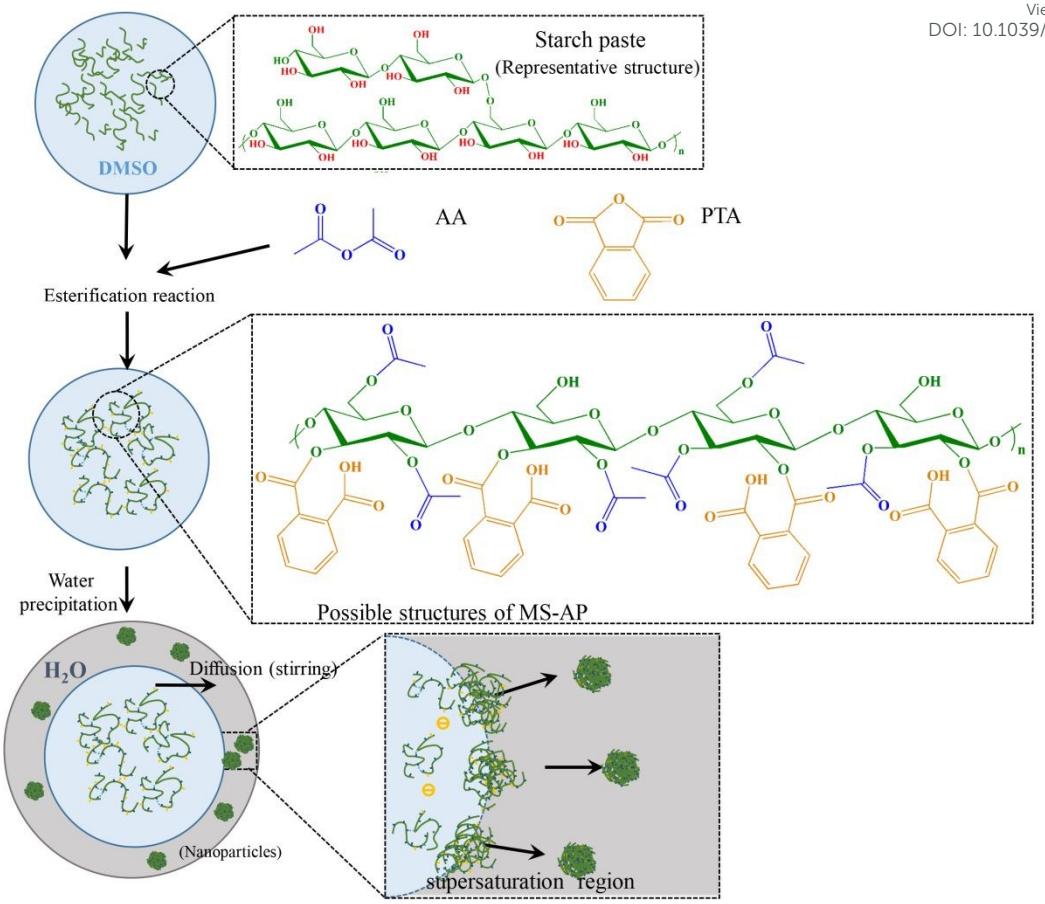

773

774 **Figure.1**

View Article Online
DOI: 10.1039/C9GC00779B

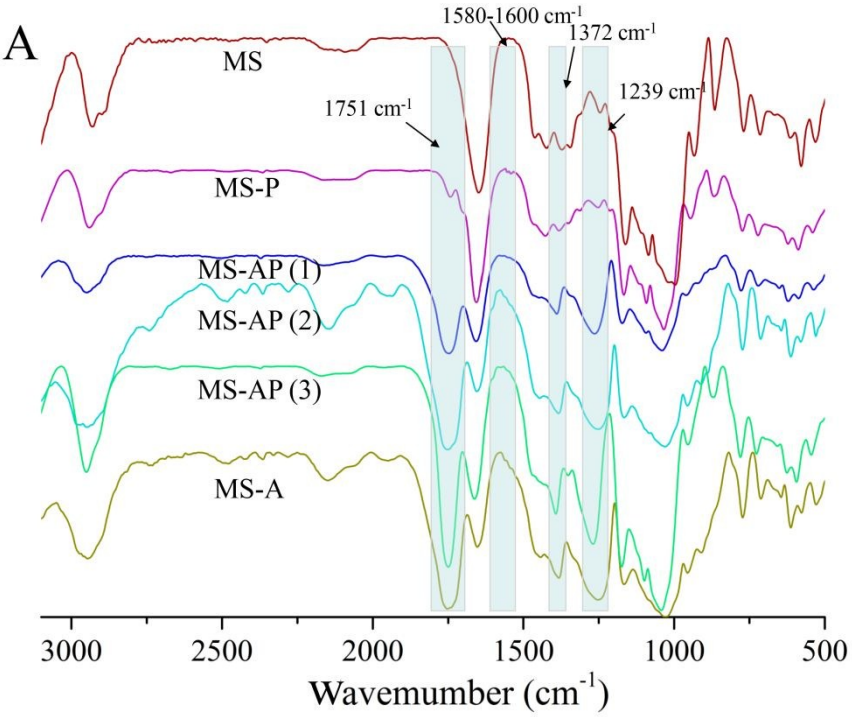

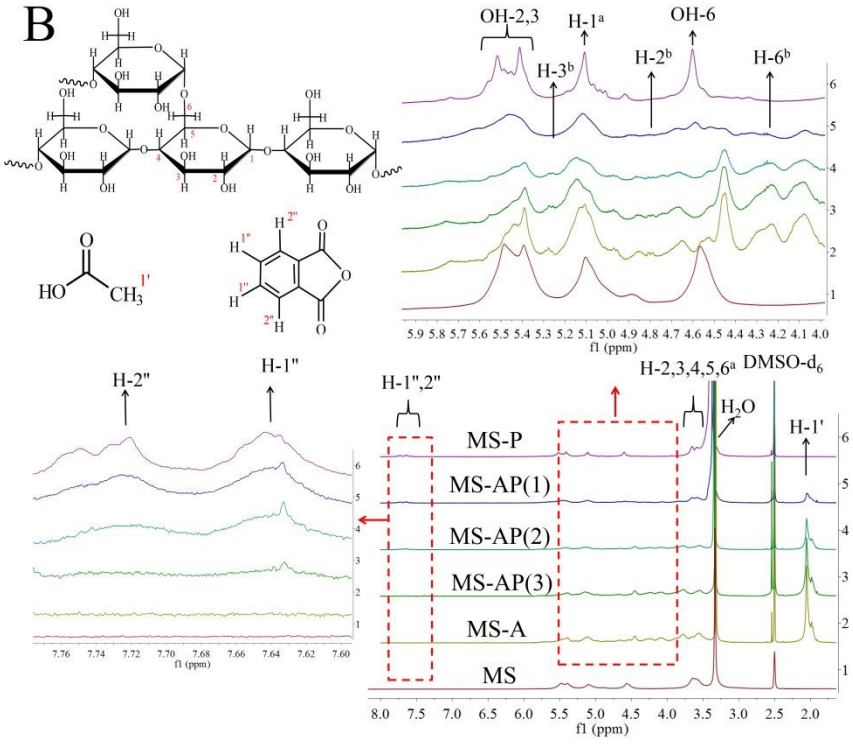

Figure.2

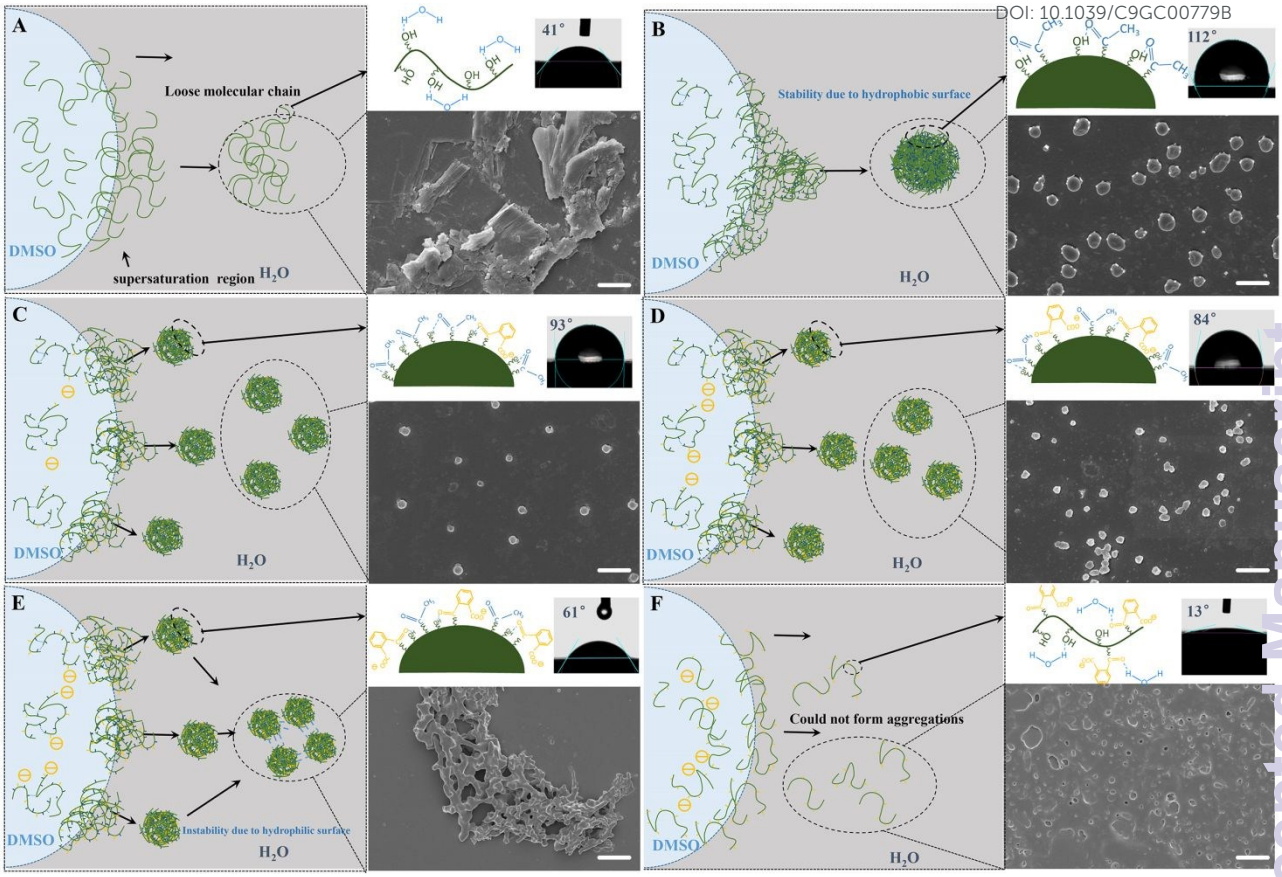

781

782 **Figure.3**

View Article Online
DOI: 10.1039/C9GC00779B

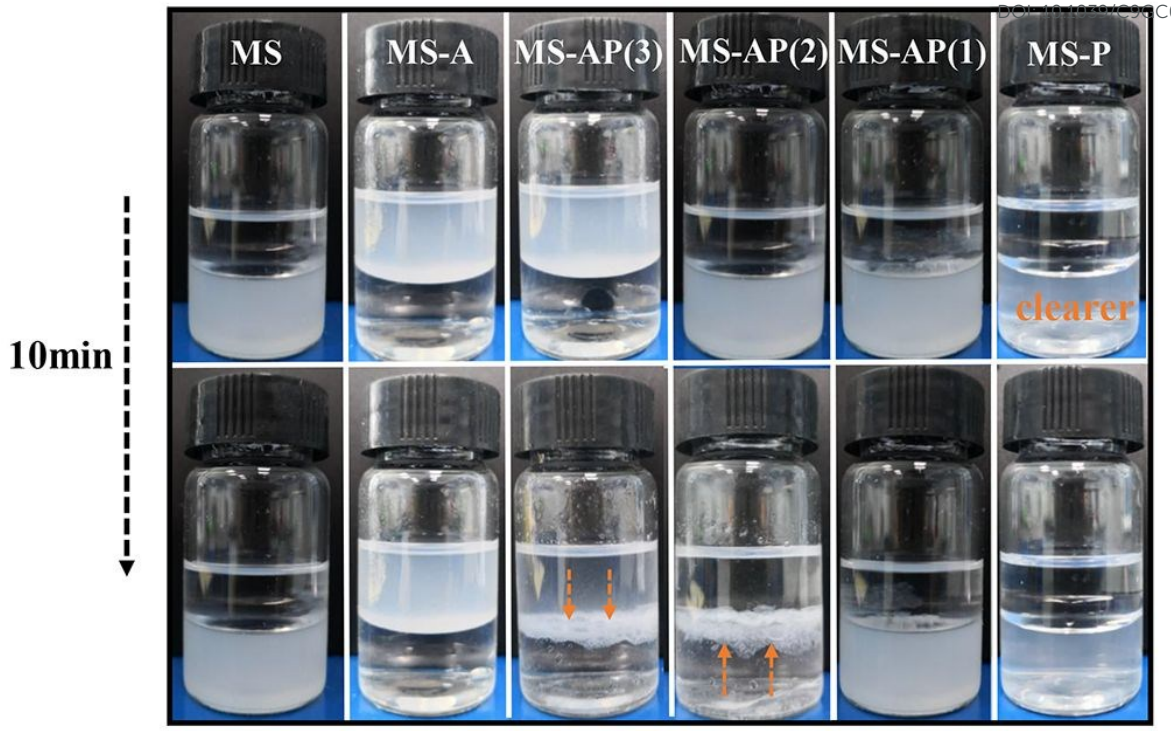

783

784 **Figure.4**

786

787 **Figure.5**

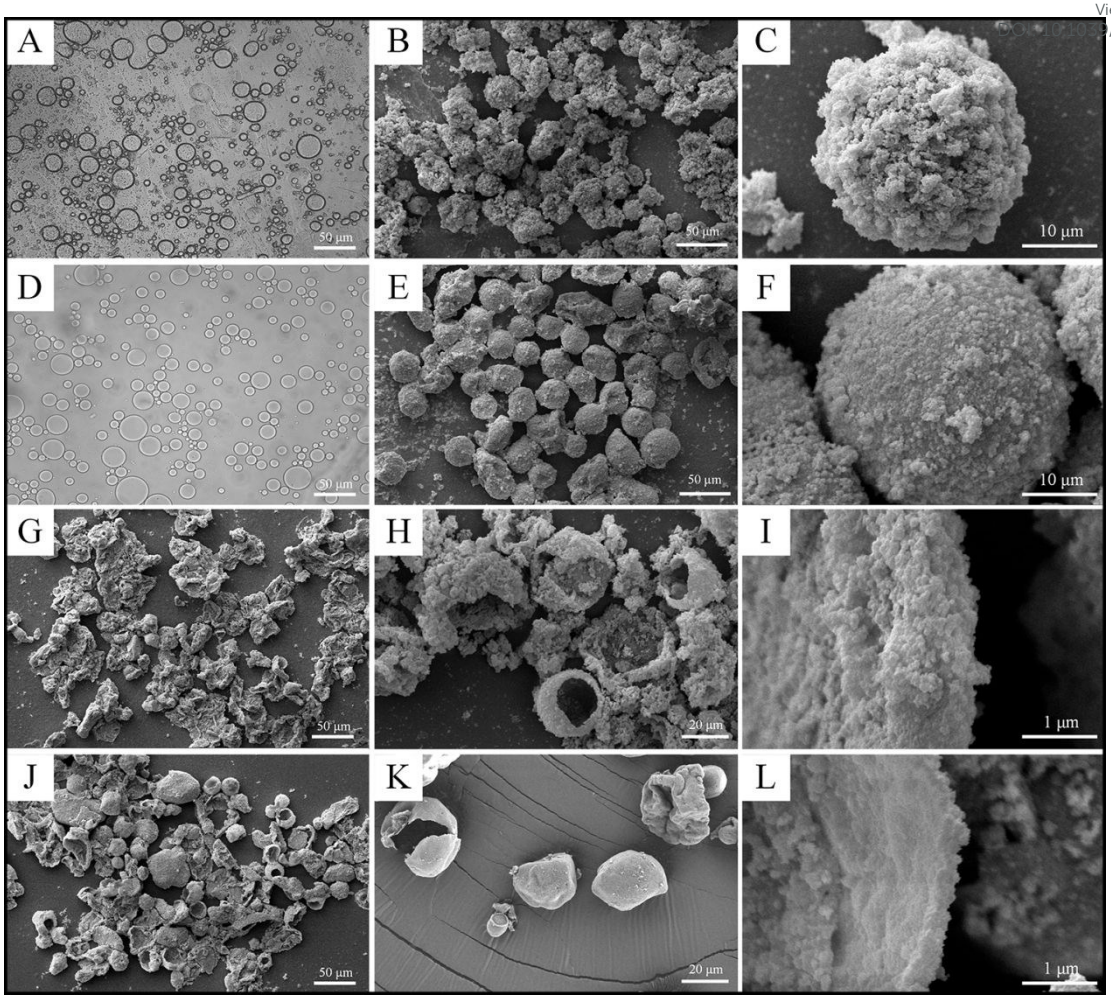

789

790 **Figure.6**

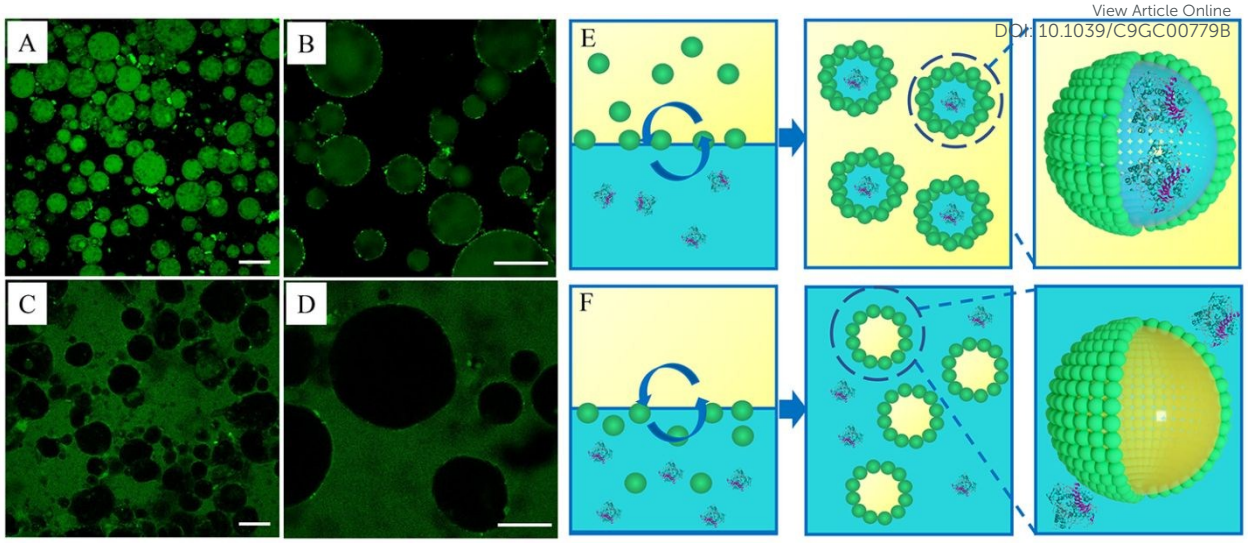

792

793 **Figure.7**

View Article Online
DOI: 10.1039/C9GC00779B

795

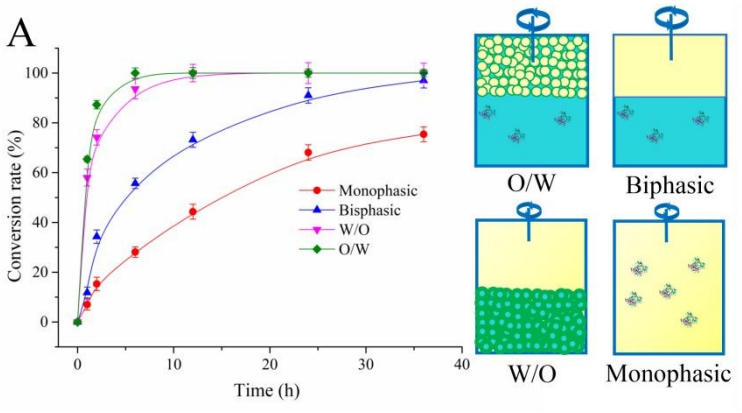

796

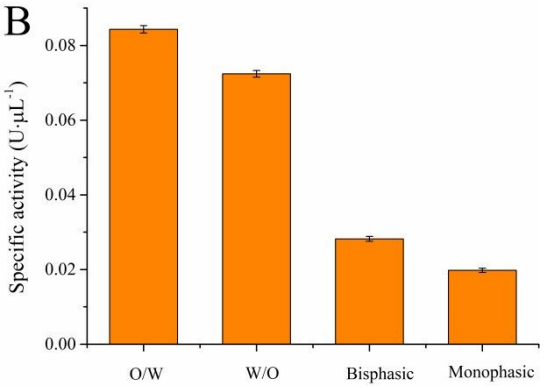

797

Figure.8

View Article Online
DOI: 10.1039/C9GC00779B

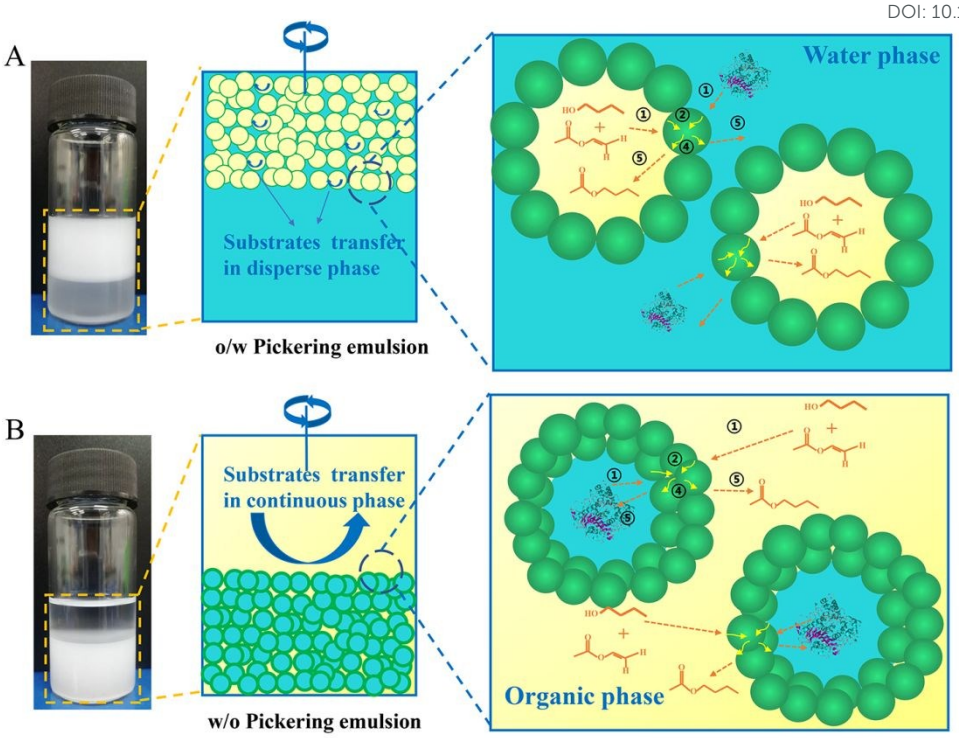

799

800 **Figure.9**

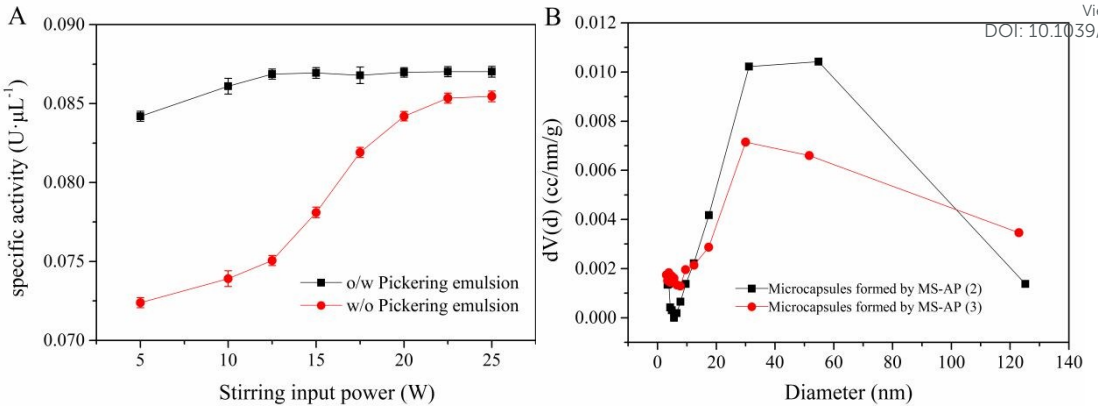

801

802 **Figure.10**

View Article Online
DOI: 10.1039/C9GC00779B

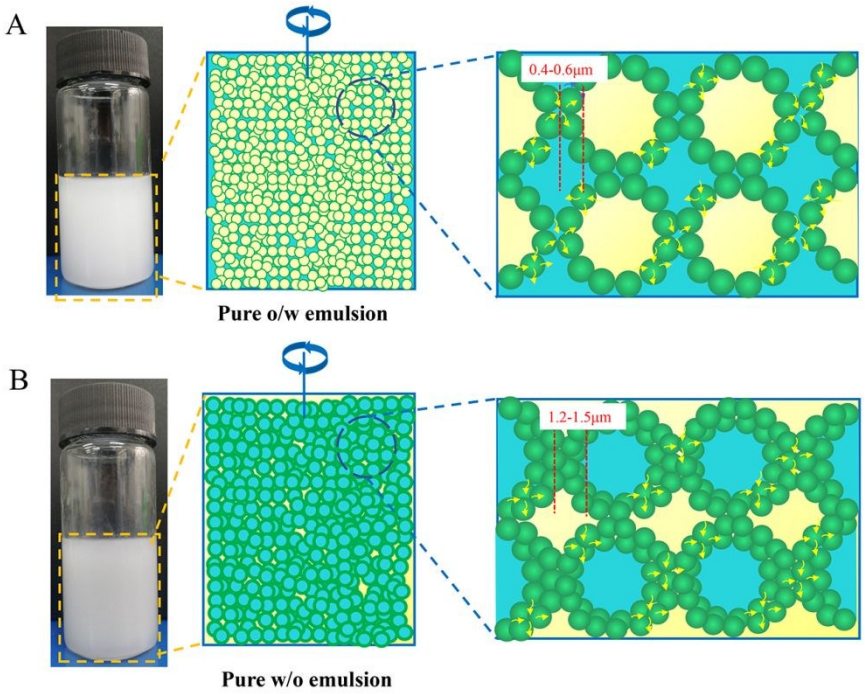

804

805 **Figure.11**

View Article Online
DOI: 10.1039/C9GC00779B

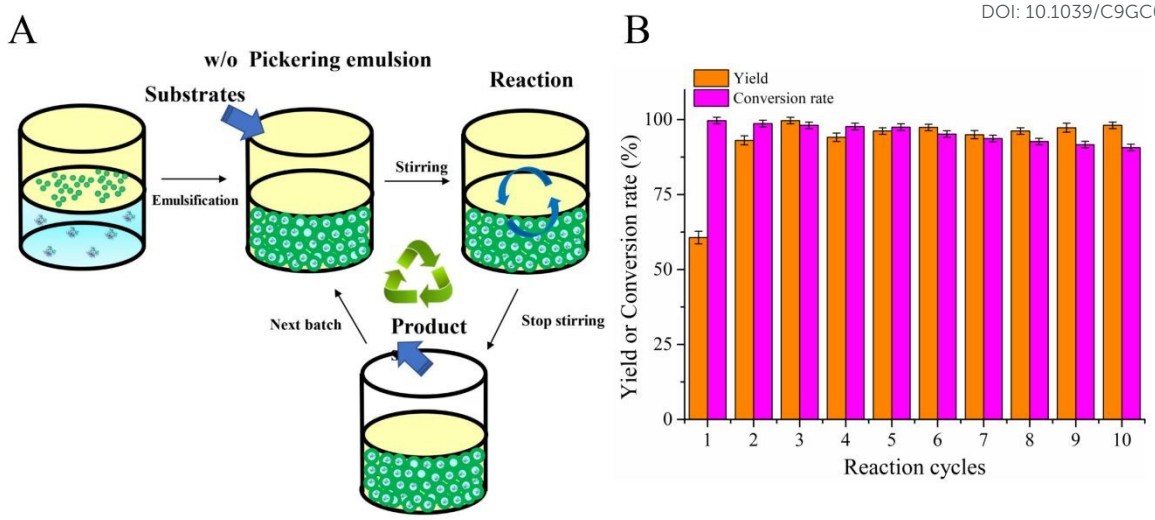

807

808 **Figure.12**

View Article Online
DOI: 10.1039/C9GC00779B

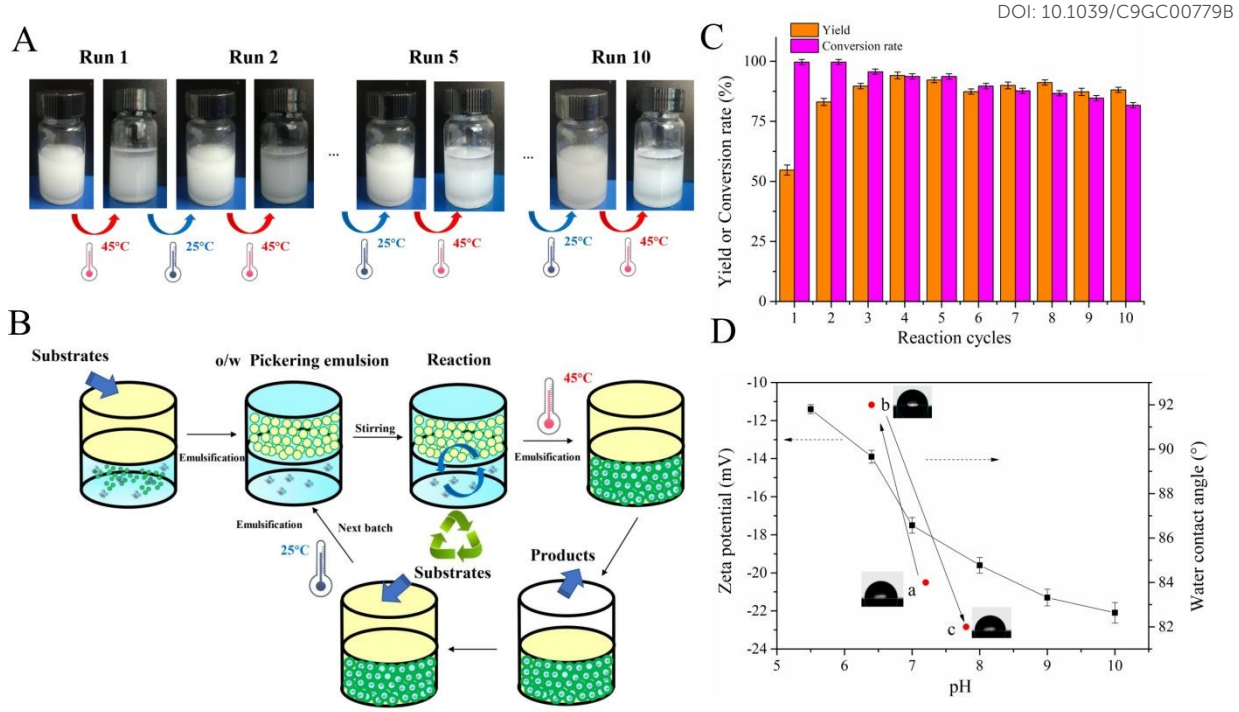

Figure.13